

AWARD NUMBER: W81XWH-13-1-0439

TITLE: Alpha2-Adrenergic Receptors and Breast Tumor Stroma: A Novel Pathway Driving Breast Cancer Growth and Metastasis

PRINCIPAL INVESTIGATOR: Kelley S. Madden, PhD

CONTRACTING ORGANIZATION: University of Rochester
Rochester, NY 14611-3847

REPORT DATE: October 2014

TYPE OF REPORT: Annual

PREPARED FOR: U.S. Army Medical Research and Materiel Command
Fort Detrick, Maryland 21702-5012

DISTRIBUTION STATEMENT: Approved for Public Release;
Distribution Unlimited

The views, opinions and/or findings contained in this report are those of the author(s) and should not be construed as an official Department of the Army position, policy or decision unless so designated by other documentation.

REPORT DOCUMENTATION PAGE				Form Approved OMB No. 0704-0188	
Public reporting burden for this collection of information is estimated to average 1 hour per response, including the time for reviewing instructions, searching existing data sources, gathering and maintaining the data needed, and completing and reviewing this collection of information. Send comments regarding this burden estimate or any other aspect of this collection of information, including suggestions for reducing this burden to Department of Defense, Washington Headquarters Services, Directorate for Information Operations and Reports (0704-0188), 1215 Jefferson Davis Highway, Suite 1204, Arlington, VA 22202-4302. Respondents should be aware that notwithstanding any other provision of law, no person shall be subject to any penalty for failing to comply with a collection of information if it does not display a currently valid OMB control number. PLEASE DO NOT RETURN YOUR FORM TO THE ABOVE ADDRESS.					
1. REPORT DATE October 2014		2. REPORT TYPE Annual		3. DATES COVERED 30 Sep 2013 - 29 Sep 2014	
4. TITLE AND SUBTITLE Alpha2-Adrenergic Receptors and Breast Tumor Stroma: A Novel Pathway Driving Breast Cancer Growth and Metastasis				5a. CONTRACT NUMBER	
				5b. GRANT NUMBER W81XWH-13-1-0439	
				5c. PROGRAM ELEMENT NUMBER	
6. AUTHOR(S) Kelley S. Madden, PhD E-Mail: Kelley_Madden@urmc.rochester.edu				5d. PROJECT NUMBER	
				5e. TASK NUMBER	
				5f. WORK UNIT NUMBER	
7. PERFORMING ORGANIZATION NAME(S) AND ADDRESS(ES) University of Rochester 910 Genesee St. Ste 200 Rochester, NY 14611-3847				8. PERFORMING ORGANIZATION REPORT NUMBER	
9. SPONSORING / MONITORING AGENCY NAME(S) AND ADDRESS(ES) U.S. Army Medical Research and Materiel Command Fort Detrick, Maryland 21702-5012				10. SPONSOR/MONITOR'S ACRONYM(S) U.S. Army Medical Research and Materiel Command Fort Detrick, Maryland 21702-5012	
				11. SPONSOR/MONITOR'S REPORT NUMBER(S)	
12. DISTRIBUTION / AVAILABILITY STATEMENT Approved for Public Release; Distribution Unlimited					
13. SUPPLEMENTARY NOTES					
14. ABSTRACT Breast cancer metastasis is facilitated by sympathetic nervous system (SNS) activation, but the role for α 2-AR, a major class of SNS receptors, has not been elucidated. The goal of this proposal is to characterize the effects of dexmedetomidine (DEX), a highly selective α 2-AR agonist, on tumor metastasis in preclinical models of breast cancer. We tested the hypothesis that α 2-AR-induced tumor progression is mediated by alterations in fibrillar collagen microstructure as detected by multiphoton second harmonic generation (SHG) imaging. Using 4T1, a metastatic mammary adenocarcinoma in BALB/c mice, α 2-AR activation increased metastasis to the lungs in conjunction with elevated tumor SHG-emitting collagen. DEX did not alter metastasis or tumor SHG in immunodeficient BALB/c SCID mice or in MMTV-PyMT mice. In BALB/c mice treated with a β 2-AR-selective agonist, increased 4T1 metastasis was also associated with elevated SHG-emitting collagen. These results suggest 1) increased collagen SHG is indicative of elevated metastatic risk; 2) DEX acts via functional T cells to alter collagen SHG; and 3) the effect of DEX may be dependent on the tumor model. At the low, non-sedative dose used here, DEX did not alter sympathetic neurotransmission, confirming that DEX acts through peripheral, post-synaptic α 2-AR to modify tumor collagen. Tumor associated fibroblasts (TAF) were isolated to determine if α 2-AR activation directly modulates collagen microstructure.					
15. SUBJECT TERMS Alpha2-adrenergic receptors, breast cancer, metastasis, dexmedetomidine, collagen, tumor associated fibroblasts, second harmonic generation					
16. SECURITY CLASSIFICATION OF:			17. LIMITATION OF ABSTRACT	18. NUMBER OF PAGES	19a. NAME OF RESPONSIBLE PERSON
a. REPORT	b. ABSTRACT	c. THIS PAGE			USAMRMC
Unclassified	Unclassified	Unclassified	Unclassified	24	19b. TELEPHONE NUMBER (include area code)

Table of Contents

	<u>Page</u>
1. Introduction.....	4
2. Keywords.....	4
3. Accomplishments.....	4
4. Impact.....	23
5. Changes/Problems.....	23
6. Products.....	23
7. Participants & Other Collaborating Organizations.....	23
8. Special Reporting Requirements.....	n/a
9. Appendices.....	none

1. INTRODUCTION

Despite advances in the treatment of breast cancer, metastatic disease remains a challenging clinical problem with few therapeutic options (1). Patients undergoing diagnosis and treatment of breast cancer often experience severe and chronic psychological stress. The sympathetic nervous system (SNS) is an important pathway by which psychological stress can promote tumor progression (2, 3). The SNS neurotransmitters norepinephrine (NE) and epinephrine activate two major classes of adrenergic receptors (AR), α -AR (subdivided into α_1 and α_2) and β -AR (subdivided into β_1 , β_2 , and β_3). The pro-tumor pathways activated by β -AR stimulation have been elucidated in breast and other cancers (4, 5), but there is a paucity of studies examining a role for α -AR activation, despite the fact that in human breast cancers, α -AR expression has been linked to poor prognosis (6). Few tumor cell lines have been demonstrated to express functional α -AR, but the host stromal cells that make up a tumor, including macrophages and fibroblasts, express α -AR and β -AR normally (7-9) and in primary tumors (10). Here we describe progress made in defining the impact of α_2 -AR activation using a highly metastatic breast cancer cell line in BALB/c mice, 4T1. 4T1 cells (and the luc2-transfected 4T1 line used here) do not express functional β -AR or α_2 -AR and cannot directly respond to the endogenous neurotransmitter NE (11), making 4T1 an excellent model for evaluating the impact of SNS activation and release of NE on host stromal cells in the absence of direct AR activation of the tumor cells. Here we describe progress made in defining the impact of α_2 -AR activation in BALB/c and BALB/c SCID mice bearing 4T1 mammary tumors and in MMTV-PyMT mice that spontaneously develop metastatic mammary tumors. We also report on companion research implicating β -AR activation in the context of 4T1.

2. KEYWORDS

breast cancer, metastasis, alpha2-adrenergic receptors, beta-adrenergic receptors, dexmedetomidine, salmeterol, tumor associated fibroblasts, collagen, second harmonic generation, multiphoton laser scanning microscopy

3. ACCOMPLISHMENTS

What were the major goals of the project?

(The specific aims are the major goals of this project. The months in parentheses are taken from the approved SOW and indicate the time frame under which each goal will be begun and completed.)

Aim 1. Determine if α_2 -AR-induced tumor progression and metastasis is a biological pathway common to many murine breast tumor models. (Months 3-20). Progress reported below.

Aim 2. Identify the cellular and molecular mechanism(s) underlying α_2 -AR-induced tumor progression within 4T1 tumors. (Months 3-16). Progress reported below.

Aim 3. Determine if DEX treatment during breast tumor surgery promotes micrometastasis. (Months 6-22). No progress to report.

What was accomplished under these goals?

Describe 1) major activities; 2) specific objectives; 3) significant results or key outcomes, including major findings developments or conclusions (both positive and negative); and/or 4) other achievements.

SPECIFIC AIM 1

1) Major activities: For specific aim 1, we assessed the effect of DEX treatment in BALB/c, BALB/c SCID, and MMTV-PyMT mice. In BALB/c and BALB SCID mice, IVIS imaging was conducted in mice bearing d-luciferase transfected 4T1 tumor cells and *ex vivo* in metastatic organs.

2) Progress was made in each of the following specific objectives:

- 1a.** Determine if α_2 -AR activation by DEX increases tumor growth and metastases in spontaneous and injectable preclinical breast cancer models. (BALB/c, BALB/c SCID, MMTV-PyMT)
- 1b.** Determine if increased SHG-emitting collagen is a marker of α_2 -AR-induced metastasis in tumor and in metastatic sites. (BALB/c, BALB/c SCID, MMTV-PyMT)
- 1c.** Identify tumor cytokines/chemokines altered by α_2 -AR stimulation. (BALB/c, BALB/c SCID, MMTV-PyMT)
- 1d.** Determine if presynaptic 'autoinhibitory' α_2 -AR are activated by DEX treatment. (MMTV-PyMT mice only)

3) Significant results/key outcomes:

We have previously reported that DEX treatment increased 4T1 tumor growth and metastasis to the lung in BALB/c mice (11). To determine if metastasis to sites other than the lung, we used IVIS imaging in BALB/c mice to compare tumor growth measured manually using calipers to IVIS imaging over time. We also measured tumor SHG F/B ratio, in conjunction with multianalyte and cellular analyses to elucidate the mechanisms underlying the effects of DEX. Finally, to determine if the response to α_2 -AR activation is dependent on mature T cells, we tested the effects of DEX in BALB/c SCID mice that lack mature T cells. We demonstrate here the following key findings:

Materials and Methods.

Drug Treatment. Mice were injected intraperitoneally (IP) with sterile saline or 10 μ g/kg DEX beginning 2 days prior to injection of 2×10^5 tumor cells into a mammary fat pad and continuing daily until the day before sacrifice. In these experiments, mice were sacrificed 18 d post 4T1 injection.

Tumor Growth. Tumor diameter was measured using calipers as described in (11).

IVIS Imaging. In BALB/c mice, luc2-transfected-4T1 cells (Caliper Life Sciences) were employed to image tumor growth *in vivo*. For IVIS imaging, mice were injected IP with luciferin (Caliper; 150 mg/kg) in sterile saline. Five minutes later, mice were anesthetized using 90 mg/kg ketamine plus 10 mg/kg xylazine. Mice were placed in the heated (37°C) imaging chamber. Imaging time was set to autoexposure to minimize the number of saturated pixels. In initial experiments, we also attempted to image distant metastatic sites, but had little success blocking the light emitted by the tumor when the tumor was large. We therefore used *ex vivo* imaging at sacrifice to image distant sites. For *ex vivo* imaging, mice were injected with 150 mg/kg luciferin and sacrificed by pentobarbital overdose 5 minutes later. Tissues (lung and bone) were dissected for immediate IVIS imaging using autoexposure.

SHG Imaging. The method for determining the F/B ratio of a thin tissue sample has been previously described (12). Briefly, a Spectra Physics MaiTai Ti:Sapphire laser (power=0.1 mW for all imaging) was directed through an Olympus Fluoview FV300 scanner. This was focused through an Olympus water-immersion lens (20 \times , 0.95 NA), which subsequently captured backward propagating SHG signal. The SHG signal was separated from the excitation beam using a 670 nm dichroic mirror, filtered using a 405 nm filter, and collected by a photomultiplier tube. The forward scattered SHG was collected through an Olympus 0.9 NA condenser, reflected by a 565 nm dichroic mirror to remove excitation light, filtered by a 405 nm filter, and captured by a photomultiplier tube. Forward- and backward-scattered SHG images were simultaneously collected as a stack of 11 images spaced 3 μ m apart with a 660- μ m field of view. For each tissue section, 5 F/B images were collected (one in the center and 4 equi-distant points around the periphery of the section) and the average F/B ratio was calculated for each section. During acquisition of all SHG images, a dilute FITC fluorescein isothiocyanate solution was imaged to calibrate for day-to-day fluctuations in laser power.

Flow cytometry. Single cell suspensions were prepared and incubated with antibodies conjugated to different fluorophores: anti-CD45-blue violet; anti-CD11b-Alexafluor 647; anti-F4/80-FITC; anti-Gr-1-phycoerythrin. Color compensation was incorporated into all analyses. Negative controls were based on fluorescent minus one (FMO) background staining. For FMO autofluorescence, cells are incubated with all fluorophores except one, and the fluorescence intensity of the missing fluorophore was determined. The myeloid cell markers were gated based on CD45+ leukocytes. CD45 is a marker of all hematopoietic cells and is not expressed by tumor cells or fibroblasts.

Lung metastasis. Paraffin-embedded formalin-fixed lung tissue was sectioned into 5-micron sections. Three serial sections were mounted onto each slide and stained using hematoxylin and eosin (H&E). Five sets of serial sections were taken from each lung, 100 μ m distance between each set. This spacing allows us to survey metastatic lesions throughout the lung. A blinded observer determined the number of metastasis in each section using a brightfield microscope (4x–20x magnification). The average number of lesions per three consecutive lung sections was calculated. This average was used to calculate the sum total of metastatic lesions in five sections per lung.

Statistical Analysis. Statistical analysis for all experiments was conducted with GraphPad PRISM software with $p < 0.05$ considered statistically different. Outliers were determined using the Grubbs method and excluded from further analyses. In experiments with two experimental groups, an F-test for variance was conducted. If the variance was similar between groups ($p > 0.05$), an unpaired, two-tailed student's t-test was employed. If the F-test for variance was significant ($p < 0.05$), group comparisons were conducted using the non-parametric Mann-Whitney U-test. For analysis of tumor growth over time, tumor volume was analyzed using repeated measure ANOVA. Significant main effects were analyzed by Holm-Sidak multiple comparison test.

A. DEX Treatment in BALB/c and BALB/c SCID mice

1. Tumor growth, metastasis, and SHG-emitting collagen in BALB/c mice (Objective 1a)

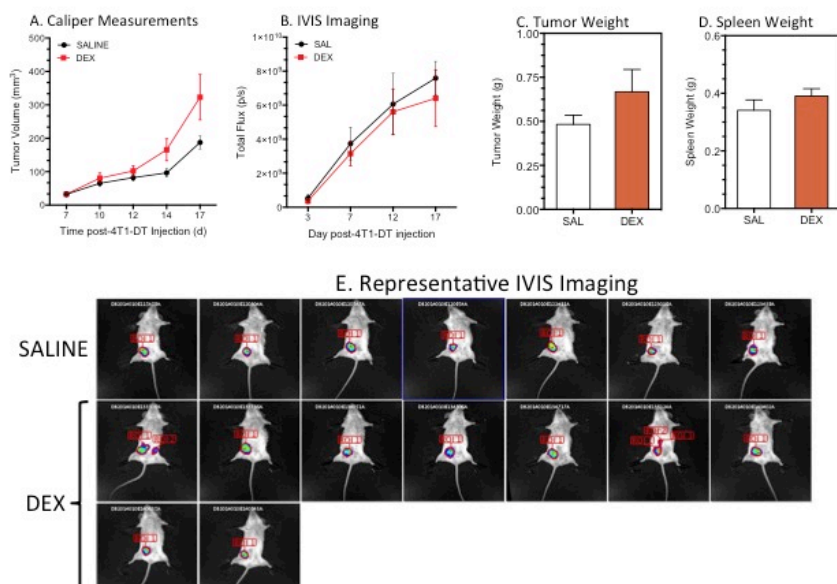


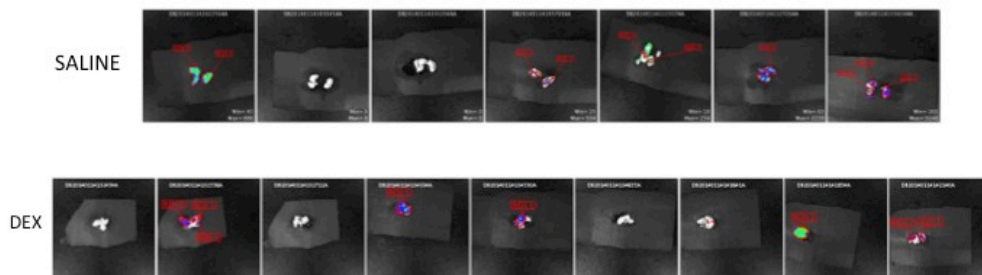
Fig. 1. 4T1 tumor growth in BALB/c female mice. A. Tumor volume calculated using caliper measures. B. Total flux from ROIs determined from images represented in E. C. Tumor weight and D. spleen weight at sacrifice, d 18 post-4T1 injection. Results expressed as mean \pm SEM. See text for statistical analysis.

In BALB/c mice, DEX treatment non-significantly increased tumor volume (Fig. 1A; repeated measures ANOVA, DEX \times time interaction, $p = 0.08$; main effect of DEX treatment, $p = 0.13$). However, this increased tumor volume was not observed with IVIS imaging as measured by total flux (photons/second) (Fig. 1B). (Representative IVIS imaging at d12 post-4T1 injection with regions of interest is shown in Fig. 1E.) Neither tumor nor spleen weights differed significantly between saline and DEX-treated mice at sacrifice (Fig. 1C,D).

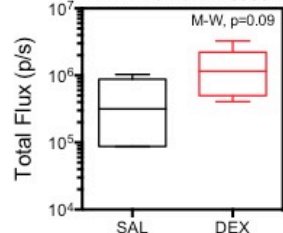
Ex vivo IVIS imaging of lungs is shown in Fig. 2A. (In this experiment, no other distant site had a detectable luminescent signal.) Based on the *ex vivo* imaging, the number of mice with detectable lung metastasis in saline-treated mice (5/7 lungs; 71.4%) did not differ significantly from DEX-treated mice (5/9 lungs; 43%) based on Fisher's chi square analysis. In those lungs with detectable luminescence, there was a trend towards increased total flux in the DEX-treated mice (Fig. 2B;

Mann-Whitney U test, $p=0.09$), suggesting larger metastatic lesions. However, in H&E-stained lung tissue sections, the number of metastatic lesions was not altered by DEX treatment (Fig. 2C; t-test, $p=0.4$). Furthermore, by H&E staining, 6/7 mice in the saline-treated groups had detectable metastasis and 9/9 mice had detectable metastatic lesions in the DEX-treated group, a frequency of detection that was not observed

A. Ex Vivo IVIS Imaging of Lungs



B. Ex Vivo Luminescence



C. H&E Stained

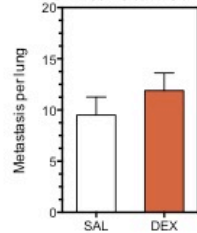


Fig. 2. Lung metastasis in DEX-treated BALB/c mice. A. Ex vivo imaging of lungs. B. Total flux measured in ROIs in A. Mann-Whitney (M-W) U test, $p=0.09$. C. Number of metastasis per lung as determined in H&E stained lung sections. Results expressed in B as median, minimum and maximum response and in C as mean \pm SEM.

with IVIS imaging. The reason for this discrepancy may be due to the fact that with *ex vivo* IVIS imaging we are capturing only a certain proportion of tumor cells on or near the surface of the tumor. With H&E analysis, the number of metastases per lung was estimated by quantifying the number of metastatic lesion in 5 tissue slices distributed equally through the lung. By *ex vivo* IVIS imaging, no metastasis was detectable in bone marrow in BALB/c mice. This result and the ambiguity of the metastatic data in the lungs suggest that later time points after tumor cell injection need to be tested to assess metastasis to additional distant metastatic site in immune-intact BALB/c mice.

2. SHG imaging (objective 1b).

We have demonstrated that changes in tumor collagen microstructure detected by measuring SHG correlates with distant metastasis in mouse breast cancer models and in breast cancer patients (12, 13). To assess the changes in the fibrillar collagen microstructure with DEX treatment, SHG forward scattered to back scattered emission (the F/B ratio) was measured in tumors as described in materials and methods. Tumor F/B was elevated in DEX-treated compared to saline-treated mice (Fig. 3A). Representative images are shown in Fig. 3B. The planned immunohistochemical analysis of total collagen type I could not be done in experiments using the luc2-transfected 4T1 cells, due to the fact the tumor cells were co-transfected with d-tomato, a bright red fluorescent protein that interfered with epifluorescent imaging of the collagen. To determine if the changes in SHG-emitting collagen were associated with alterations in extracellular matrix modifiers, tumor matrix metalloproteinases (MMPs) and transforming growth factor-beta (TGF- β) were measured in tumor homogenates (14). DEX treatment did not alter tumor MMP-2, -3, and pro-MMP-9 (Fig. 4A-C) or total or active TGF- β (Fig. 4D,E). In future experiments we will assess MMP-1 and -13, MMPs that directly modify collagen type I. We should also point out that we were not satisfied with the quality of the TGF- β ELISA used for these experiments, and the different forms of TGF- β were not distinguishable with this ELISA. In future experiments, we will use the TGF- β 1, -2, and -3 multiplex bead-based kit available through Millipore.

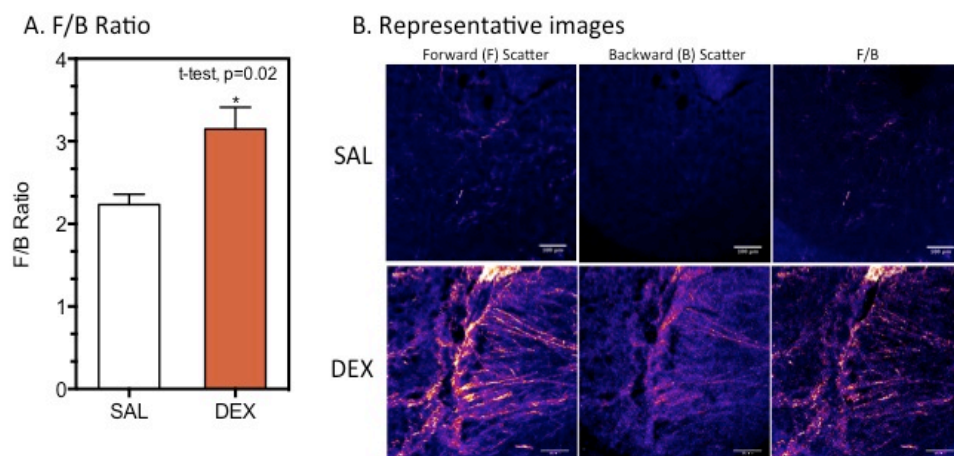


Fig. 3. Second harmonic generation (SHG) imaging of 4T1 tumor fibrillar collagen in BALB/c mice. A. Tumor F/B ratio is increased in mice treated with dexmedetomidine (DEX) compared to saline (SAL); t-test, $p=0.02$; B. Representative images of tumor SHG scattered in the forward (F) and backward (B) direction. The F/B image was produced by dividing the original gray-scale F scatter image by the B scatter image using Image J. The images shown here were false-colored. Images were taken with a 20X objective lens using 1X electronic zoom. Scale bars = 100 μ m.

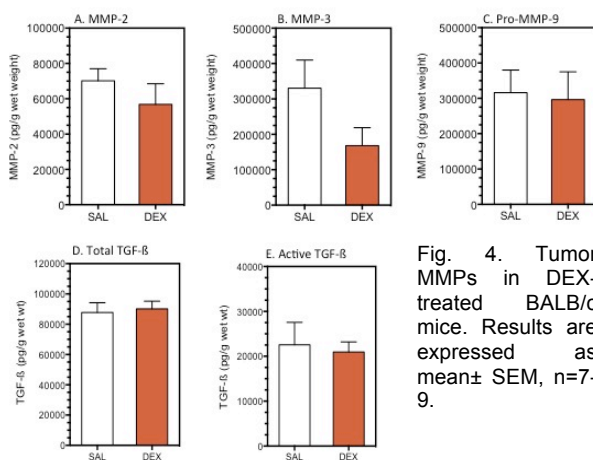


Fig. 4. Tumor MMPs in DEX-treated BALB/c mice. Results are expressed as mean \pm SEM, $n=7-9$.

Tumor cytokines/chemokines and myeloid cell populations (objective 1c).

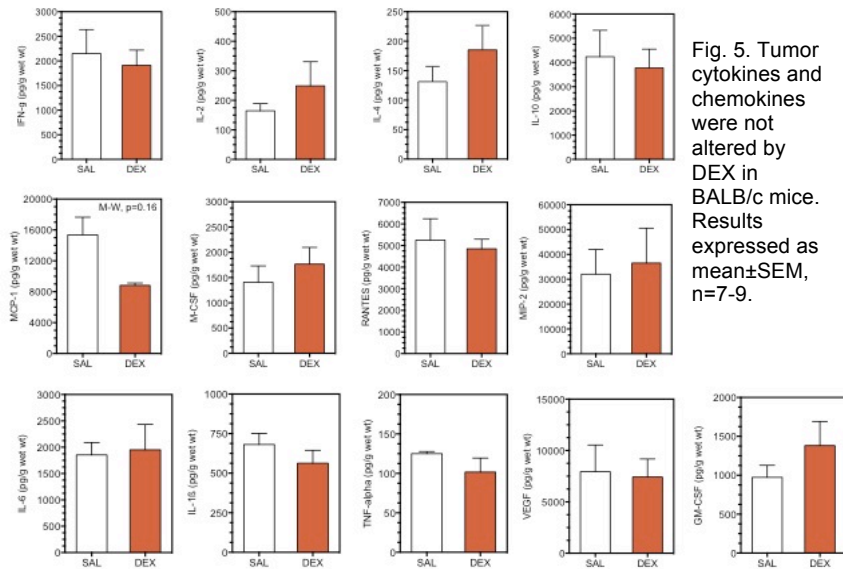


Fig. 5. Tumor cytokines and chemokines were not altered by DEX in BALB/c mice. Results expressed as mean±SEM, n=7-9.

To further examine mechanisms underlying the DEX-induced increase in SHG F/B ratio, cytokines and chemokines in tumor homogenates were tested in a multianalyte bead-based multiplex kit (Millipore). DEX treatment did not significantly alter immune cell-derived cytokine, including IFN- γ , IL-2, IL-4, or IL-10, proinflammatory cytokines IL-6, IL-1 β or TNF- α , chemokines MCP-1 (CCL-2), M-CSF (CSF-1), RANTES (CCL-5), MIP-2, or VEGF and GM-CSF (Fig. 5). Myeloid cell populations were also assessed

in tumor and in spleen based on flow cytometric analysis of the myeloid cell surface markers CD11b, F4/80 and Gr-1. Representative staining of these populations in tumor cells (Fig. 6) and spleen cells (Fig. 7) is shown. In DEX-treated mice, a trend towards increased CD45+ leukocytes was detected in the tumors from DEX-treated mice (Fig 8A), and in the spleen, the frequency of CD45+ leukocytes increased significantly (Fig 8B). However, DEX treatment did not alter the frequency of tumor or splenic myeloid cell populations (Fig. 8A,B). The DEX-induced increase in the CD45+ population suggests that DEX treatment may have increased T cells, but T cell frequency was not assessed in this experiment.

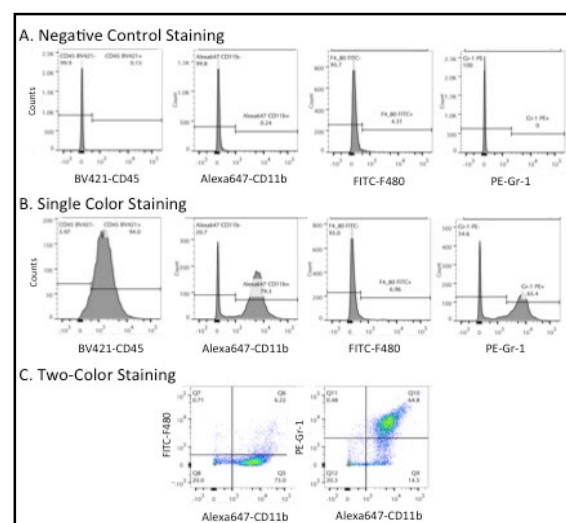
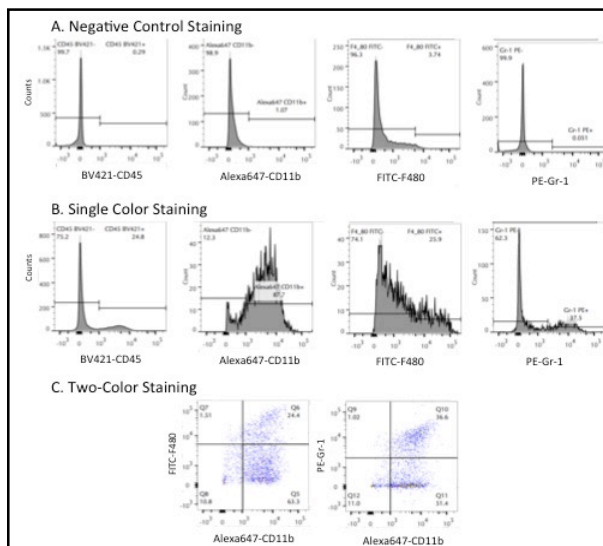


Fig 6 (left) and Fig. 7 (right). Flow cytometric analysis of tumor (left) and spleen (right) cells for myeloid markers CD11b, F480, and Gr-1. A. Autofluorescence (negative control staining) was determined using fluorescence minus one (FMO) controls; B. Single-color histograms of CD45+ leukocytes gated on the tumor or spleen cell population determined by SSC vs FSC bit map gating (not shown). The CD11b+, F4/80+, and Gr-1+ populations were gated on the CD45+ population, and analysis gates were set based on the negative control staining; C. Two-color histograms of CD11b versus F4/80 populations and CD11b versus Gr-1 gated on the CD45+ population. The analysis gates in the two-color histograms were set based on the single color analysis gating.

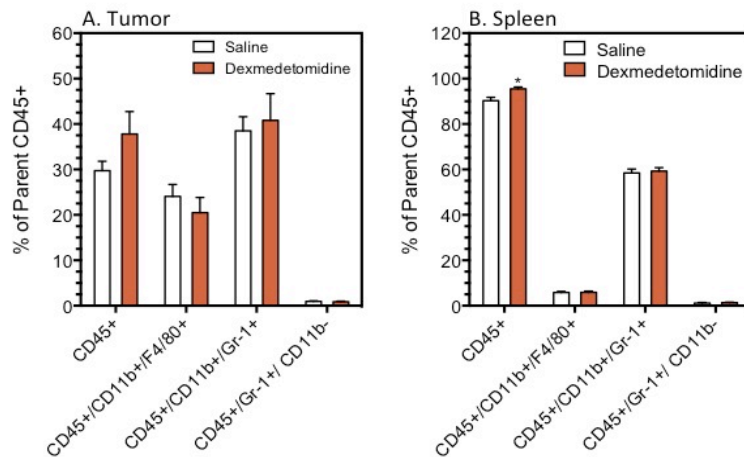


Fig. 8. Tumor (A) and spleen (B) cell population frequencies in DEX-treated BALB/c mice. DEX did not alter myeloid populations but it significantly increased CD45+ leukocytes in the spleen. * t-test, $p < 0.05$ vs saline. Results expressed as mean \pm SEM, $n = 7-9$ per group.

Discussion: DEX treatment in BALB/c Mice. Elevated DEX-induced metastasis was not readily detected in these mice as in our previous experiments (11). Here a trend towards increased cells in metastatic lung lesions in DEX-treated mice, as measured by total flux (Fig. 2B), was not confirmed by H&E analysis. Nonetheless, we observed an increase in tumor SHG-emitting collagen. In this experiment, the tumors grew more slowly compared to our previously reported experiments, and in those experiments, the DEX-induced increase was more apparent later in tumor growth (11). The animals in the current experiment were manipulated more frequently for IVIS imaging, which was not done previously. We are also concerned that the anesthesia administered for IVIS imaging may interact with DEX. For example, anesthesia (ketamine combined with xylazine, an $\alpha 2$ -AR agonist) may reduce sensitivity to DEX through $\alpha 2$ -AR desensitization (15, 16). The planned studies in other mouse strain/tumor combinations (aim 1) will help elucidate if this is a possibility, as luciferase-transfected cells and IVIS imaging will not be conducted. We plan to repeat DEX treatment in BALB/c mice with sacrifice at varying time points in tumor growth to determine when DEX-induced alterations in SHG-emitting collagen alterations appear relative to changes in tumor growth and metastasis. We will incorporate standard H&E analysis of bone marrow to determine if DEX-induced metastasis is a global effect versus a more restricted targeting of lung. If the alterations in SHG F/B ratio in BALB/c mice occur before there is a clear difference in metastasis, then SHG F/B ratio may be an early indicator of future metastatic risk.

3. Tumor growth, metastasis, SHG-emitting collagen in BALB/c SCID mice

To further investigate the cellular mechanisms underlying DEX-induced elevation of SHG-emitting collagen, we hypothesized that the DEX-induced increase in CD45+ leukocytes in the spleen (and a similar trend in the tumors) may indicate that T cells were responsive to $\alpha 2$ -AR treatment (17) and contributed to elevated tumor SHG-emitting collagen. To determine if the DEX-induced increase in tumor F/B ratio is dependent on functional T cells, 4T1 tumor-bearing BALB/c SCID mice were treated with DEX as described.

In T cell-deficient BALB/c SCID mice, DEX treatment did not significantly alter tumor volume as determined with calipers (Fig. 9A; repeated measure ANOVA, main effect $p = 0.23$). However, IVIS imaging revealed reduced tumor growth over time (Fig. 9B, repeated measure ANOVA, main effect $p = 0.03$) that was associated with a trend towards reduced tumor weight at sacrifice (Fig. 9C, t-test, $p = 0.08$). Spleen weight was not significantly altered by DEX treatment (Fig. 9D). There was no significant difference in lung metastases based on standard H&E analysis (Fig. 9E) or *ex vivo* IVIS imaging of lungs (Fig. 9F). In these immunocompromised mice, bone metastasis was detected by *ex*

vivo IVIS imaging (Fig. 10A), but no significant differences in total flux were observed in bone with

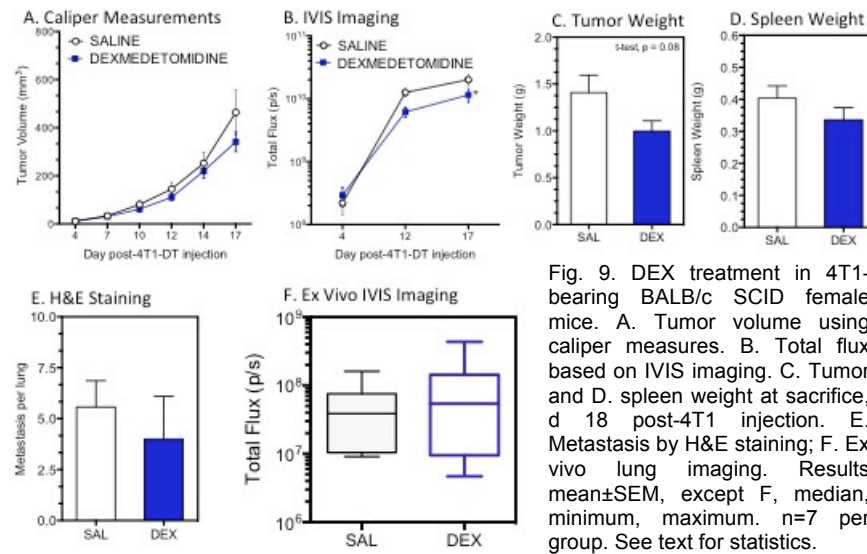


Fig. 9. DEX treatment in 4T1-bearing BALB/c SCID female mice. A. Tumor volume using caliper measures. B. Total flux based on IVIS imaging. C. Tumor and D. spleen weight at sacrifice, d 18 post-4T1 injection. E. Metastasis by H&E staining; F. Ex vivo lung imaging. Results mean \pm SEM, except F, median, minimum, maximum. n=7 per group. See text for statistics.

DEX treatment (Fig. 10B). Unlike in BALB/c mice, DEX treatment did not alter tumor SHG F/B ratio in BALB/c SCID mice (Fig. 11).

In association with reduced tumor growth, DEX treatment significantly reduced tumor MMP-2 (Fig. 12A), but not MMP-3 (Fig. 12B) pro-MMP-9 (Fig. 12C), or the active form of TGF- β (Fig. 12D). DEX treatment also significantly reduced tumor IL-10, but not any other chemokine or cytokine (Fig. 13).

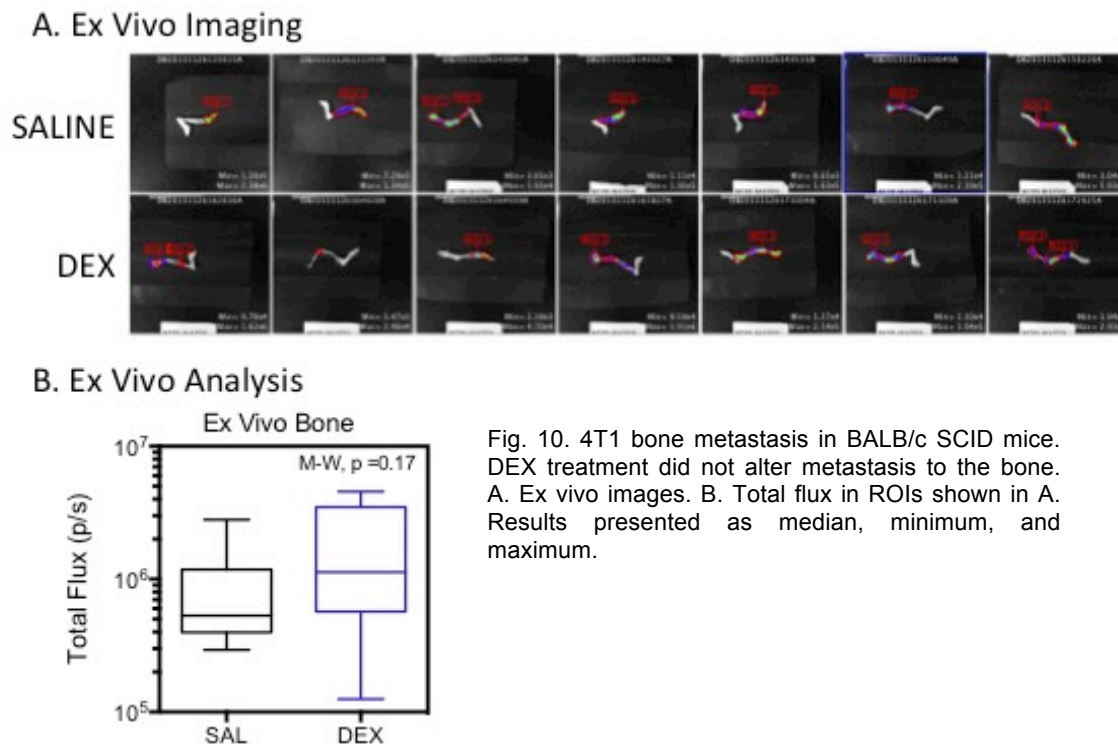


Fig. 10. 4T1 bone metastasis in BALB/c SCID mice. DEX treatment did not alter metastasis to the bone. A. Ex vivo images. B. Total flux in ROIs shown in A. Results presented as median, minimum, and maximum.

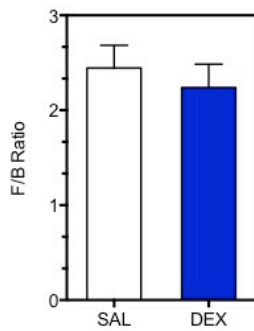


Fig. 11. SHG imaging of 4T1 tumor fibrillar collagen in BALB/c SCID mice. Results expressed as mean \pm SEM, n=7 per group.

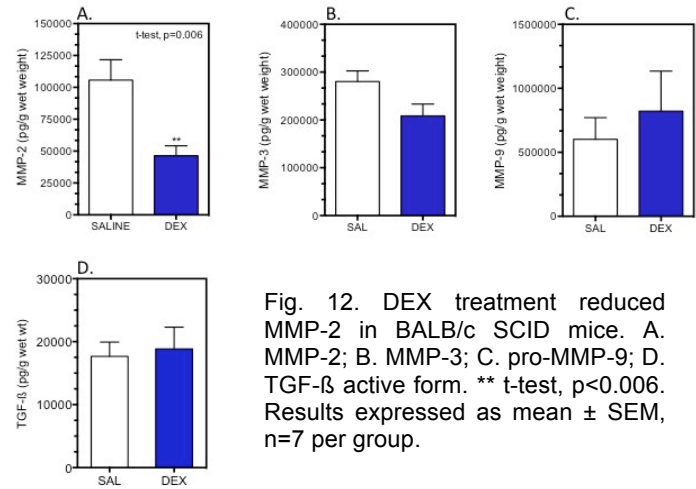


Fig. 12. DEX treatment reduced MMP-2 in BALB/c SCID mice. A. MMP-2; B. MMP-3; C. pro-MMP-9; D. TGF-β active form. ** t-test, $p < 0.006$. Results expressed as mean \pm SEM, n=7 per group.

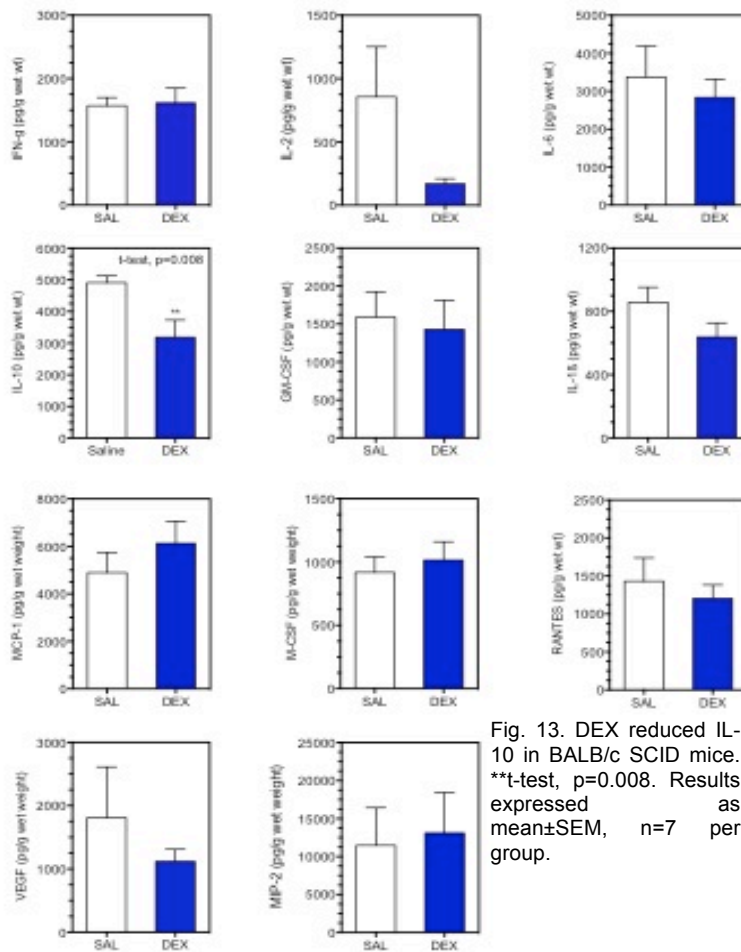


Fig. 13. DEX reduced IL-10 in BALB/c SCID mice. ***t-test, $p = 0.008$. Results expressed as mean \pm SEM, n=7 per group.

Summary of significant results (DEX treatment in BALB/c & BALB/c SCID mice). In BALB/c mice, DEX treatment elevated tumor SHG F/B ratio when there were trends possibly indicative of increased growth and metastasis, but no clear increase in these measures as we reported previously (11). DEX did not increase tumor growth, metastasis or tumor SHG F/B ratio in BALB/c SCID mice, indicating that the presence of functional T cells are necessary for α 2-AR agonist-induced alterations in SHG-emitting collagen. Furthermore, alterations in the tumor SHG F/B ratio in BALB/c mice was not associated with alterations in myeloid populations or in tumor cytokines or chemokines associated with these populations. MMP-2, -3, and pro-MMP-9 and TGF- β , important proteins associated with modification of the extracellular matrix, were not altered by DEX treatment. These results indicate that α 2-AR activation may modify fibrillar collagen structure through other mechanisms, such as alterations in adhesion molecule expression or fibroblast collagen production. These possibilities are currently being tested (see specific aim 2 progress below).

In BALB/c SCID mice, DEX-induced inhibition of tumor growth in conjunction with reduced MMP-2 is indicative of an α 2-AR-mediated tumor inhibitory pathway that is not apparent in the presence of functional T cells. Despite the inhibition of tumor growth, metastasis to lungs and bone did not appear altered with DEX treatment in BALB/c SCID mice. Therefore this finding will not be pursued further in the context of this project.

B. DEX treatment in the Spontaneous Mammary Tumor Model MMTV-PyMT

We tested if DEX altered tumor progression in MMTV-PyMT mice, a transgenic line that spontaneously develops invasive mammary tumors that metastasize to the lungs (18). The goal of this experiment was to 1) characterize the response to DEX in a spontaneous preclinical breast cancer model (objective 1a), and 2) to determine if the α 2-AR altered sympathetic neurotransmission as measured by the sympathetic neurotransmitter norepinephrine (NE) and its metabolite, normetanephrine, in the spleen (objective 1d).

Materials and Methods.

DEX treatment. MMTV-PyMT mice were treated with 10 μ g/kg DEX IP daily beginning at 9 weeks of age when mammary tumors were in the early carcinoma phase and when metastasis to the lungs was not detectable. The injections continued for 2 weeks, and mice were sacrificed at 11 weeks of age when tumors had entered the late carcinoma/invasive phase and metastatic lesions were detectable in the lungs.

Tumor Growth and Lung Metastasis. Tumor burden was measured by determining the total weight of mammary tumors dissected from each mouse. The number of lung metastasis was determined using H&E staining as described above.

Tissue NE and NMN. Portions of the spleen and tumor were homogenized in 0.1 N HCl. NE and NMN in the homogenate were measured by ELISA (Rocky Mountain Diagnostics) and normalized to wet weight of the tissue.

Results. DEX treatment did not reduce tumor burden (Fig. 14A) or lung metastasis (Fig. 14B) in MMTV-PyMT mice in conjunction with no alterations in tumor SHG-emitting collagen (Fig. 14C). Of the tumor cytokines and chemokines measured, non-significant alterations in IL-12p70, IFN- γ , and TNF- α were noted (Fig. 14D). MMPs and TGF- β were not measured in this experiment. To determine if DEX treatment altered sympathetic neurotransmission, NE and its metabolite normetanephrine (NMN) were measured in tumor and spleen. We have previously observed that spleen NE and NMN are good measures of SNS activation, while tumors are less so (11, 19), therefore NE and NMN were measured in both tissues. Neither spleen nor tumor NE or NMN were significantly altered by DEX treatment (Fig. 14E, F). By flow cytometric analysis, DEX did not alter the frequency of CD45⁺ cells or the myeloid populations described above (data not shown).

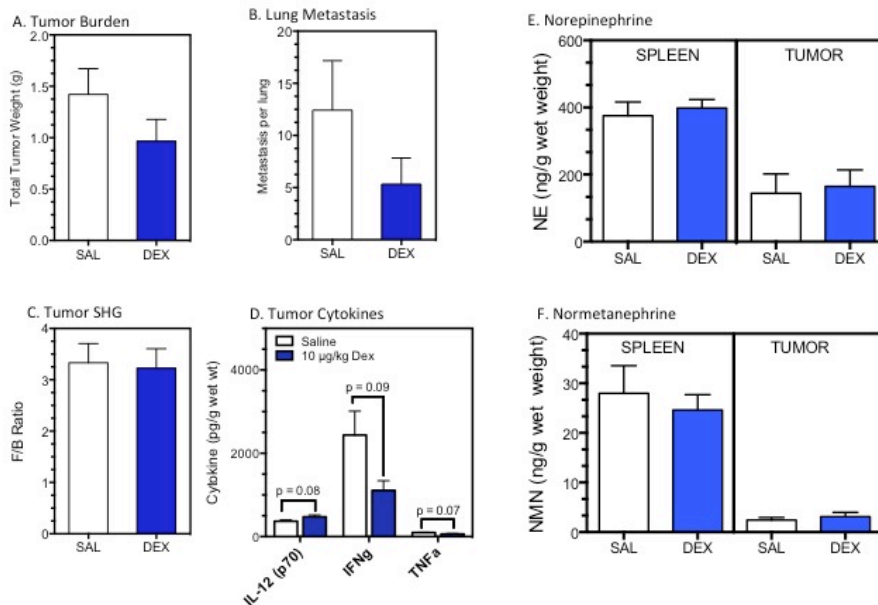


Fig. 14. DEX treatment in MMTV-PyMT mice. DEX treatment did not alter tumor pathogenesis as measured by A. tumor burden (t-test, $p=0.19$); B. number of lung metastasis (M-W, $p=0.3$); C. tumor SHG F/B ratio. D. Trends in tumor cytokines indicated by student's t-test. E, F. DEX did not alter spleen or tumor E. NE or F. NMN. Results expressed as mean \pm SEM, $n=6$ mice per group.

Discussion/Summary of Significant Results (DEX in MMTV-PyMT mice). DEX treatment did not alter tumor growth or metastasis in MMTV-PyMT mice. Correspondingly, DEX did not alter tumor SHG F/B ratio in MMTV-PyMT mice. The inability to detect DEX-induced alterations in NE or NMN indicates that DEX at the low doses used here did not modify sympathetic neurotransmission, either by stimulating sympathetic regulatory centers in the central nervous system or by activation of pre-synaptic autoinhibitory α_2 -

AR in the periphery. This result implies that DEX-induced effects are most likely mediated by activation of post-ganglionic α_2 -AR targets in the periphery. However, this conclusion must be further tested in a tumor model that displays a more robust effect of DEX on tumor progression. The inability of DEX to elicit any changes in tumor growth or metastasis may suggest that DEX is effective only during specific stages in tumor progression or it may indicate that the effect of α_2 -AR activation on breast tumor progression is dependent on the breast tumor type. The MMTV-PyMT model differs in several important ways from 4T1: MMTV-PyMT mammary tumors develop spontaneously from hyperplasia to advanced, metastatic carcinoma. MMTV tumors also express estrogen and progesterone receptors (18), unlike 4T1, and AR expression of the MMTV-PyMT tumor cells has yet to be established. Thus it is possible that DEX-induced alterations in tumor progression are dependent on the molecular characteristics of the breast tumor.

Specific Aim 2

1) Major activities: Identify the cellular and molecular mechanism(s) underlying α_2 -AR-induced tumor progression within 4T1 tumors. (Months 3-16)

2) Specific objectives:

Aim 2a. Evaluate tumor associated fibroblasts as targets of α_2 -AR agonists.

Aim 2b. Evaluate the impact of tumor associated fibroblasts on collagen organization as measured by second harmonic generation.

We have initiated objective 2a under task 2 in the SOW, and the significant results are shown here.

3) Significant results/key outcomes:

Here we demonstrate the isolation of tumor associated fibroblasts (TAF) from 4T1 tumors. The goal of these experiments was to determine the optimal conditions and appropriate markers for isolation of TAF and to optimize yield and purity of the isolated cells. Fibroblast expression of 2 cell surface

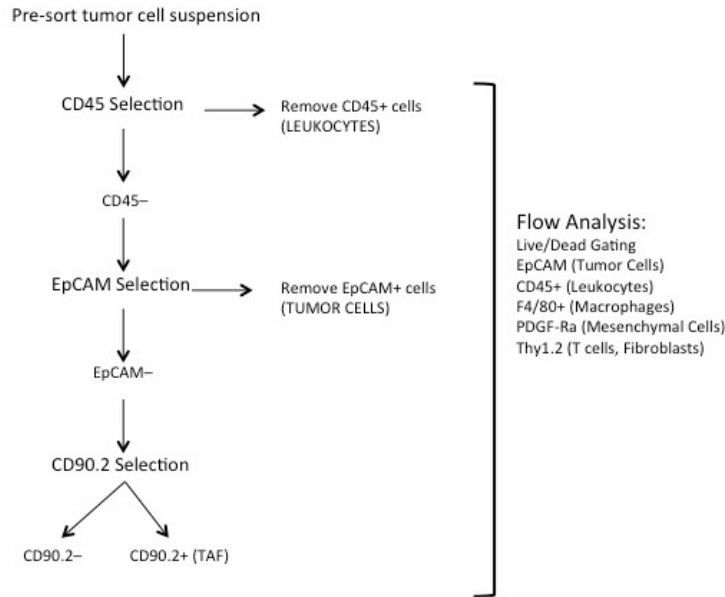


Fig. 15. Schematic representation of negative and positive selection strategy for isolating tumor associated fibroblasts.

markers associated with TAF was evaluated: platelet derived growth factor receptor-alpha (PDGF-Rα, CD140a) (20) and CD90.2 (Thy1.2) (21, 22). Flow cytometry was used to assess enrichment or depletion of different cellular populations from the tumor using the immunomagnetic selection strategy shown in Fig. 15 and described in detail below.

Materials and Methods

Preparation of Tumor Single Cell Suspensions. A protocol was developed to optimize the cell yield from each tumor. Tumors were divided into small pieces using scissors and forceps. Tumor pieces were incubated for 30 min at 37°C in a

digestion buffer containing Liberase™ (Roche; approximately 0.28 Wünsch units/ml) and DNase (100 µg/ml) with regular vortexing. The solution was passed through a 70 µm strainer, and the cells were resuspended in flow wash buffer to continue with cell selection.

Immunomagnetic cell selection. Table 1 lists antibodies/cell markers used for immunomagnetic selection using MACS cell separation columns (Miltenyi). Cells were incubated with Fc block for 15 minutes at 4°C (1:40 in MACS buffer, 1x10⁶ cells/50 µl) prior to the immunomagnetic selection procedure.

Table 1 Antibodies Used to Isolate Tumor Associated Fibroblasts

Marker	Fluorophore	Antibody	Species	Vendor
Thy1.1	PerCP-Cy5.5	Anti-mouse CD90.2	Rat	BioLegend
CD45	BV421	Anti-mouse CD45	Rat	BioLegend
PDGF-Rα	APC	Anti-mouse CD140a	Rat	BioLegend
EpCAM	Alexa Fluor 594	Anti-mouse CD326	Rat	BioLegend

The steps for isolating CD90.2+ TAF are diagrammed in Fig. 15. For CD45 depletion, 10⁷ cells were resuspended in 90 µl of MACS buffer and 10 µl anti-CD45 antibody-conjugated microbeads (Miltenyi). After vortexing, the bead-

cell suspension was incubated for 15 min at 4°C, washed, and added to a pre-rinsed LD cell separation column (Miltenyi). The column was rinsed 2 times with MACS buffer, and the effluent was collected (CD45-depleted population) for flow analysis and further cell selection.

To remove 4T1 tumor cells from the CD45-depleted population, cells were incubated with FITC-conjugated anti-CD326 (EpCAM) antibody (23), washed twice and resuspended in 500 µl of MACS buffer. The cell suspension was added to a pre-rinsed LS separation column prepared with anti-FITC antibody-conjugated microbeads. The column was rinsed 3 times and the effluent (CD45-/EpCAM-cells) was collected.

For CD90.2 (also known as Thy1.2) isolation from the effluent containing CD45-/EpCAM- cells, cells were incubated in 90 μ l MACS buffer and 10 μ l of anti-CD90.2 antibody-conjugated microbeads as described above. After washing, cells were resuspended in 500 μ l MACS buffer, and added to a pre-rinsed LS separation column. To collect the CD90.2+ cells, the separator was removed from the magnetic hold, and 5 ml of buffer pushed through column into a collection tube.

Flow Cytometric analysis. The antibodies used to characterize different cell populations are described in Table 1. The flow cytometric analysis was conducted as described above (19), except all gating was based on live cells determined with eFluor780 viability marker (eBioscience).

Results. We compared the expression of PDGFR α (CD140a) and CD90.2 (Thy 1.2) cells in small (~5-8 mm) and large (>8 mm) 4T1 tumors grown in mammary fat pads. In single cell suspensions prepared from small, 5-8 mm diameter 4T1 tumors, the percentage of live cells was 80.1% versus 19.9% dead (Fig. 16A). (The histogram in Fig. 16A was based on forward scatter vs side scatter bitmap gating, data not shown). A majority of cells obtained from unfractionated tumor cells are CD45+ leukocytes (54.1%, determined by subtracting autofluorescence (0.64%) in Fig. 16B from the CD45+ staining (54.7%) in Fig. 16C). EpCAM+ tumor cells make up 28.9% of the tumor (subtract autofluorescence in Fig. 16D (53.5%) from EpCAM staining in Fig. 16E (82.3%). F4/80+ macrophages were 19.03% (23.8-4.77) of the total tumor cell population (Fig. 16F,G). By contrast, Fig. 16H shows a small population of CD45+CD90.2+ T cells (2.54% of live cells) clearly distinguishable from a CD45-CD90.2+ population (1.72% of live cells). However, no PDGF-R α + cells were detected as a marker either co-expressed or not co-expressed with CD90.2 (Fig. 16I).

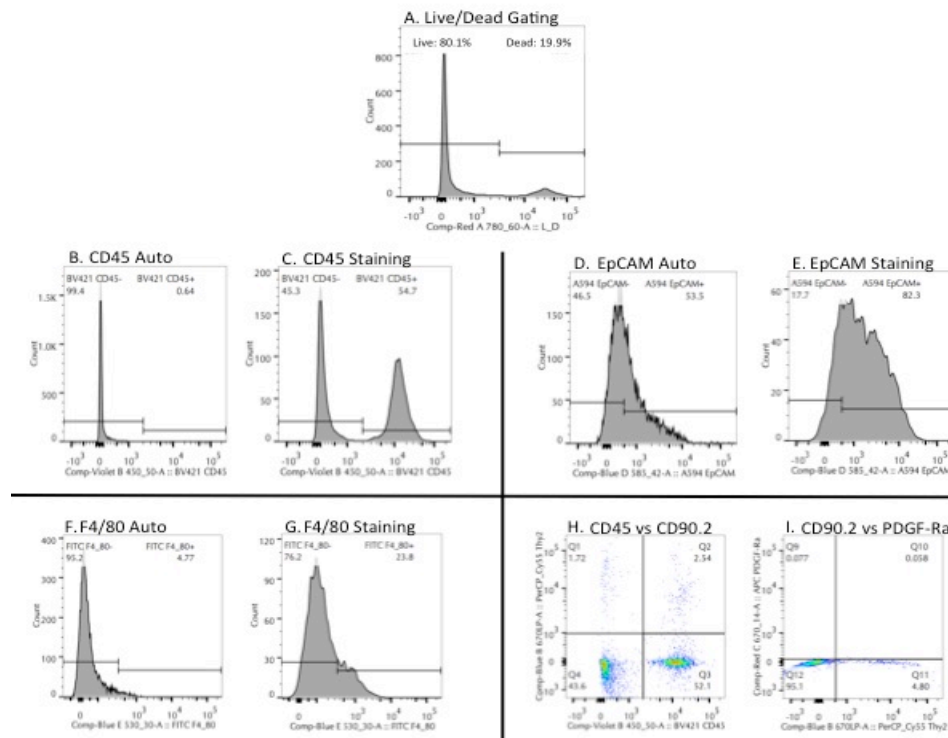


Fig. 16. Flow cytometric analysis of unfractionated cells from small 4T1 tumors. All marker staining is gated on live population indicated in A. (B,C) Autofluorescence and CD45+ frequency; (C,D) Autofluorescence and EpCAM+ frequency; (F,G) Autofluorescence and F4/80+ frequency; (H) two-color histogram CD45 versus CD90.2; (I) two-color histogram CD90.2 versus PDGF-R α .

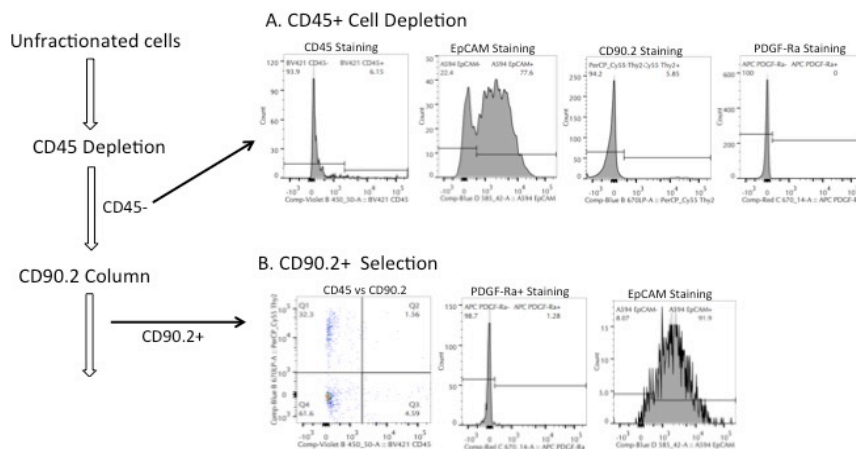


Fig. 17. Tumor cell selection using small tumors. A. CD45-depleted population evaluated for CD45, EpCAM, CD90.2 and PDGF-Ra expression. B. CD45-EpCAM- cells selected for CD90.2+ cells and evaluated for expression of CD45, PDGF-Ra, and EpCAM. (EpCAM depletion was done prior to CD90.2 selection, but results are not shown here.)

After negative selection of CD45+ cells, the percentage of contaminating CD45+ in the CD45-depleted population was 6.15% (Fig. 17A) compared to 54.1% in the unfractionated cells (Fig.16C). The CD45-depleted population was also enriched in CD90.2+ cells (5.85%) and contained a large fraction of EpCAM+ cells (77.6%) (Fig. 17A). There was no

enrichment in PDGF-Ra+ cells (0%) (Fig. 17A). (Note that in this experiment, autofluorescent controls were inadvertently omitted.) The

next step, positive selection for CD90.2+ cells from the CD45-/EpCAM- population, significantly enriched the CD45-CD90.2+ population (32.3%) with few CD45+CD90.2+ T cells (1.56%) (Fig 17B). It appeared there was a significant contamination with EpCAM+ tumor cells (Fig 17B), however, this was difficult to assess without autofluorescent controls. We concluded that 4T1 tumors possess CD45-CD90.2+ cells that were enriched by our cell selection procedure, but we noted that the cell yield was very low.

Larger tumors (9-11 mm in diameter) were grown to determine if we could increase the yield of TAF expressing CD90.2 or PDGF-Ra. In large tumors, the population of dead cells was greatly increased (Compare Fig. 18 (96.9%) to Fig. 16A (19.9%)). Gating on the unfractionated live cells revealed a significant population of PDGF-Ra+ cells (13.3-5.63 = 7.67%; Fig. 19A), but removal of CD45+ cells did not enrich the PDGF-Ra population in either the CD45-depleted cells (7.92-3.09 = 4.83; Fig. 19B) or the CD45-enriched cells (10.5-4.33 = 6.17%; Fig. 19C). Furthermore, positive selection of CD90.2+ from the CD45-/EpCAM- cells, enriched for CD90.2+ cells (Fig. 20A; 94.7-4.69 = 90%), but not for PDGF-Ra+ cells (Fig. 20B; 7.92- 5.02 = 2.9%). Here there were only a few contaminating EpCAM+ cells (Fig. 20C; 7.39-3.91 = 3.48%), indicative of good removal of 4T1 tumor cells.

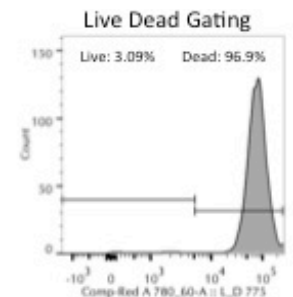


Fig. 18. Live-dead cell frequency in large 4T1 tumors.

These results demonstrate 4T1 TAF are heterogeneous with regard to expression of PDGF-Ra and CD90.2. This is consistent with the idea that tumors display a diverse population of fibroblastic cells. Based on these results, future studies will utilize 4T1 tumors ranging in size from 8-10 mm in diameter. We will further characterize the CD45-CD90.2+ fibroblasts to determine if they are α -smooth muscle actin (α -SMA) myofibroblasts (24) in conjunction with analysis of α 2-AR expression and α 2-AR-induced alterations in fibroblast function *ex vivo*.

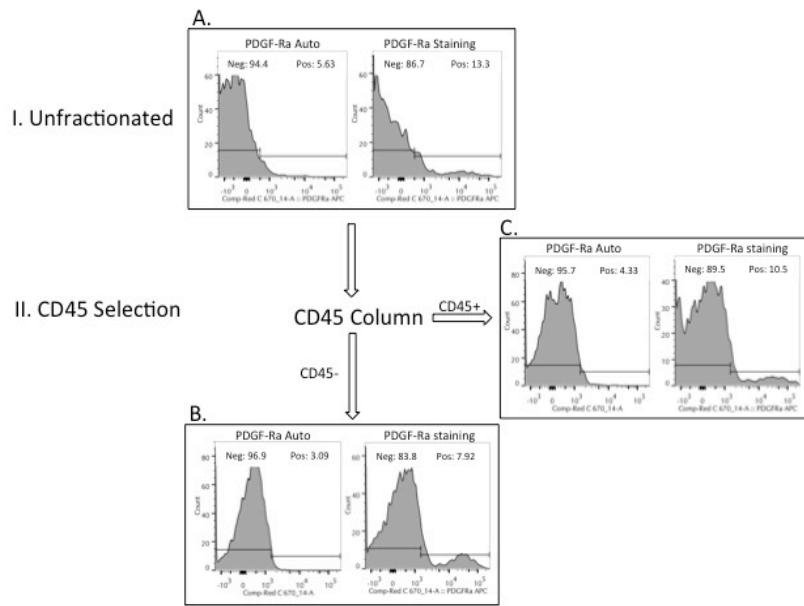


Fig. 19. PDGF-Ra expression is detectable in large tumors. PDGFRa+ cells were detectable in A. unfractionated cells; B. CD45-depleted and C. CD45-enriched populations.

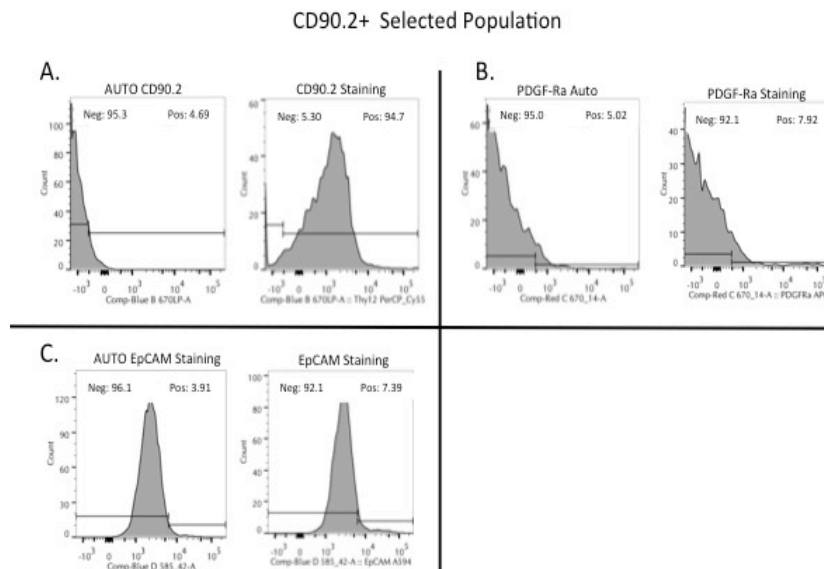


Fig. 20. In large tumors, PDGF+ cells were not significantly enriched by enrichment for CD90.2+ cells. CD90.2+ (A), but not PDGFRa+ (B) cells were enriched by positive selection for CD90.2+ cells. Note that the CD90.2-enriched population contained few contaminating EpCAM+ cells (C).

Other Significant Results/Achievements: In parallel with experiments assessing $\alpha 2$ -AR activation, we have begun to characterize the 4T1 tumor response to β -AR stimulation *in vivo*. β -AR are the other major class of AR. The rationale for testing β -AR activation in the 4T1 tumor model is the same as for utilizing 4T1 to assess the impact of $\alpha 2$ -AR activation. 4T1 cells do not express functional β -AR and do not respond to NE. β -AR activation has been shown to promote tumor progression in tumor models in which the tumor cells express functional β -AR (4, 5) but the tumor's response to β -AR activation in the absence of input from the tumor cells has not been determined. Therefore, 4T1 is an excellent model to assess the impact of β -AR activation on host β -AR-expressing stromal cells in the absence of direct input of the tumor cells.

Materials and Methods: Mice were injected IP with sterile saline or 5 mg/kg salmeterol, a long-acting highly $\beta 2$ -AR selective agonist, beginning 2 days prior to injection of 2×10^5 tumor cells into a mammary fat pad and continuing daily until the day before sacrifice, d 18 post-4T1 injection.

Results: β -AR activation reduced 4T1 tumor growth (Fig. 21A; repeated measure ANOVA, effect of salmeterol treatment, $p = 0.048$; interaction, $p = 0.18$). Salmeterol appears to have a complex effect on

metastasis with reduced metastasis to the lung occurring early in tumor development (data not shown), followed by increased metastasis to the lung later in tumor development (Fig. 21B). In conjunction with salmeterol-induced increase in the number of lung metastasis, tumor F/B ratio was elevated (Fig. 22). Tumor MMP-2, -3, and pro-9 were not significantly altered by salmeterol treatment (data not shown), but there were significant reductions in tumor IL-6 and MCP-2 (CCL2) with a significant elevation in IL-4 (Fig. 23). No other alterations in cytokines or

chemokines were detected (data not shown). In the spleen (and trending in the tumors), CD45+ leukocytes were elevated, in conjunction with reduced CD11b+Gr-1+ myeloid derived suppressor cells (MDSC) (Fig. 24). A small, but significant increase in F4/80+ macrophages was noted in the spleen, but not tumor, of salmeterol-treated mice (Fig. 24).

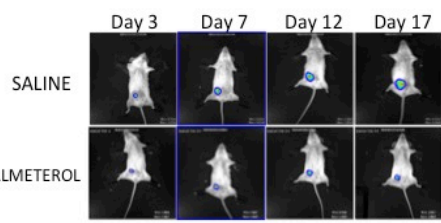
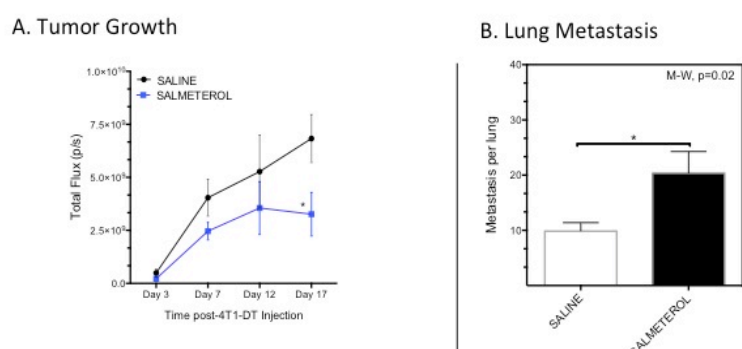


Fig. 21. $\beta 2$ -AR activation in BALB/c mice. A. IVIS imaging and representative images over time. B. Lung metastasis by H&E. A. * $p < 0.05$ at d17 by Sidak's multiple comparison B. $p = 0.02$ by Mann-Whitney. Mean \pm SEM, $n = 7$ saline, $n = 9$ salmeterol.

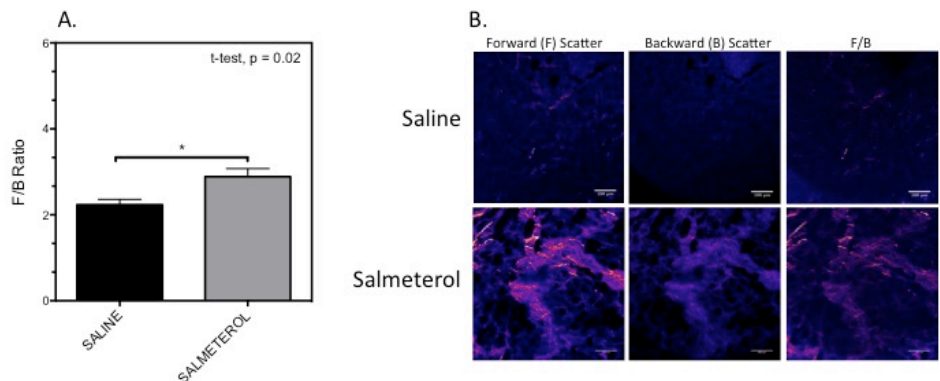


Fig. 22. $\beta 2$ -AR activation in BALB/c mice increased tumor SHG-emitting collagen. See Fig. 3 legend for details. Images were taken with a 20X objective lens using 1X electronic zoom. Scale bars = 100 μ m. Mean \pm SEM, $n = 7$ saline, $n = 9$ salmeterol.

Discussion and Significant Results ($\beta 2$ -AR activation in 4T1-bearing BALB/c mice): An association between elevated metastasis and tumor SHG F/B ratio was observed with β -AR activation, similar to that observed in the DEX-treated mice. A significant inhibitory effect of β -AR activation within the tumor microenvironment was also

revealed that has not been previously reported. These results suggest that β -AR activation of stromal cells may inhibit aspects of tumor progression and should be further explored, especially in the context of evaluating the safety of β -blockers in breast cancer patients.

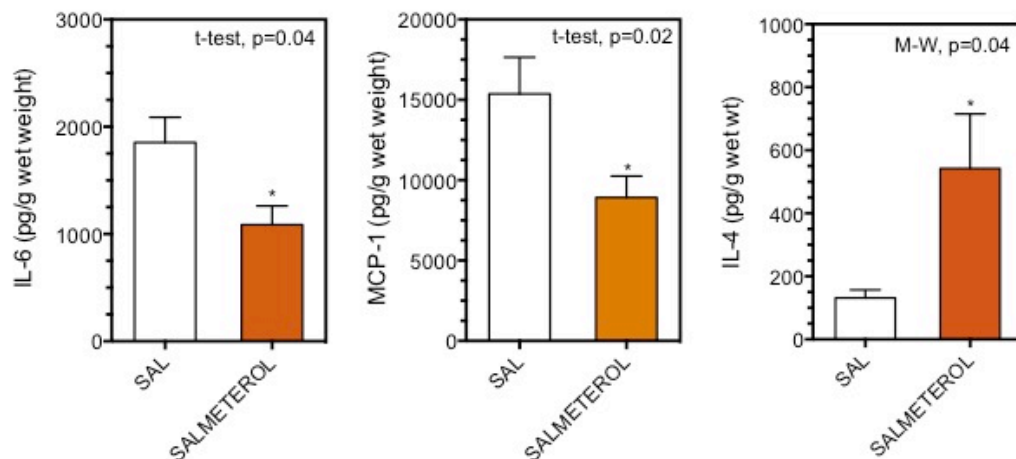


Fig. 23. Tumor cytokine and chemokine analysis in salmeterol-treated BALB/c mice. Cytokines shown (MCP-1, IL_4 and IL-6) were significantly altered by salmeterol treatment. Results shown as mean \pm SEM, n=7 saline, n=9 salmeterol.

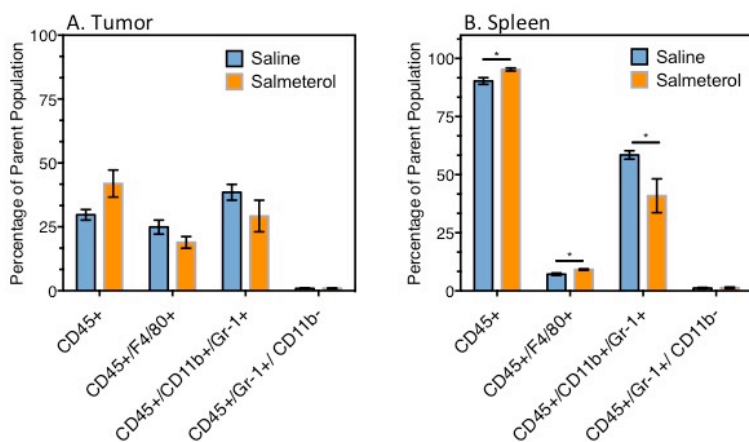


Fig. 24. Flow cytometric analysis of tumor (A) and spleen (B) myeloid populations in salmeterol-treated BALB/c mice. * t-test, p<0.05 versus saline. Results shown as mean \pm SEM, n=7 saline, n=9 salmeterol.

REFERENCES

1. Steeg PS. 2006. Tumor metastasis: mechanistic insights and clinical challenges. *Nat Med* 12: 895-904
2. Antoni MH, Lutgendorf SK, Cole SW, Dhabhar FS, Sephton SE, McDonald PG, Stefanek M, Sood AK. 2006. The influence of bio-behavioural factors on tumour biology: pathways and mechanisms. *Nat Rev Cancer* 6: 240-8
3. Cole SW, Sood AK. 2012. Molecular pathways: beta-adrenergic signaling in cancer. *Clin Cancer Res* 18: 1201-6
4. Thaker PH, Han LY, Kamat AA, Arevalo JM, Takahashi R, Lu C, Jennings NB, Armaiz-Pena G, Bankson JA, Ravoori M, Merritt WM, Lin YG, Mangala LS, Kim TJ, Coleman RL, Landen CN, Li Y, Felix E, Sanguino AM, Newman RA, Lloyd M, Gershenson DM, Kundra V, Lopez-Berestein G, Lutgendorf SK, Cole SW, Sood AK. 2006. Chronic stress promotes tumor growth and angiogenesis in a mouse model of ovarian carcinoma. *Nat Med* 12: 939-44
5. Sloan EK, Priceman SJ, Cox BF, Yu S, Pimentel MA, Tangkanangnukul V, Arevalo JM, Morizono K, Karanikolas BD, Wu L, Sood AK, Cole SW. 2010. The sympathetic nervous system induces a metastatic switch in primary breast cancer. *Cancer Res* 70: 7042-52
6. Powe DG, Voss MJ, Habashy HO, Zanker KS, Green AR, Ellis IO, Entschladen F. 2011. Alpha- and beta-adrenergic receptor (AR) protein expression is associated with poor clinical outcome in breast cancer: an immunohistochemical study. *Breast Cancer Res Treat* 130: 457-63
7. Wang Q, Lu R, Zhao J, Limbird LE. 2006. Arrestin serves as a molecular switch, linking endogenous alpha2-adrenergic receptor to SRC-dependent, but not SRC-independent, ERK activation. *J Biol Chem* 281: 25948-55
8. Spengler RN, Allen RM, Remick DG, Strieter RM, Kunkel SL. 1990. Stimulation of alpha-adrenergic receptor augments the production of macrophage-derived tumor necrosis factor. *J Immunol* 145: 1430-4
9. Nance DM, Sanders VM. 2007. Autonomic innervation and regulation of the immune system (1987-2007). *Brain Behav Immun* 21: 736-45
10. Bruzzzone A, Pinero CP, Rojas P, Romanato M, Gass H, Lanari C, Luthy IA. 2011. alpha(2)-Adrenoceptors enhance cell proliferation and mammary tumor growth acting through both the stroma and the tumor cells. *Curr Cancer Drug Targets* 11: 763-74
11. Szpunar MJ, Burke KA, Dawes RP, Brown EB, Madden KS. 2013. The antidepressant desipramine and alpha2-adrenergic receptor activation promote breast tumor progression in association with altered collagen structure. *Cancer Prev Res* 6: 1262-72
12. Burke K, Tang P, Brown E. 2013. Second harmonic generation reveals matrix alterations during breast tumor progression. *J Biomed Opt* 18: 31106
13. Burke RM, Madden KS, Perry SW, Zettel ML, Brown EB, 3rd. 2013. Tumor-associated macrophages and stromal TNF-alpha regulate collagen structure in a breast tumor model as visualized by second harmonic generation. *J Biomed Opt* 18: 86003
14. Pickup MW, Laklai H, Acerbi I, Owens P, Gorska AE, Chytil A, Aakre M, Weaver VM, Moses HL. 2013. Stromally derived lysyl oxidase promotes metastasis of transforming growth factor-beta-deficient mouse mammary carcinomas. *Cancer Res* 73: 5336-46
15. Baumann MH, Milchanowski AB, Rothman RB. 2004. Evidence for alterations in alpha2-adrenergic receptor sensitivity in rats exposed to repeated cocaine administration. *Neuroscience* 125: 683-90

16. Jewell-Motz EA, Liggett SB. 1996. G protein-coupled receptor kinase specificity for phosphorylation and desensitization of alpha2-adrenergic receptor subtypes. *J Biol Chem* 271: 18082-7
17. Felsner P, Hofer D, Rinner I, Porta S, Korsatko W, Schauenstein K. 1995. Adrenergic suppression of peripheral blood T cell reactivity in the rat is due to activation of peripheral α_2 -receptors. *J Neuroimmunol* 57: 27-34
18. Lin EY, Jones JG, Li P, Zhu L, Whitney KD, Muller WJ, Pollard JW. 2003. Progression to malignancy in the polyoma middle T oncoprotein mouse breast cancer model provides a reliable model for human diseases. *Am J Pathol* 163: 2113-26
19. Madden KS, Szpunar MJ, Brown EB. 2011. beta-Adrenergic receptors (beta-AR) regulate VEGF and IL-6 production by divergent pathways in high beta-AR-expressing breast cancer cell lines. *Breast Cancer Res Treat* 130: 747-58
20. Erez N, Truitt M, Olson P, Arron ST, Hanahan D. 2010. Cancer-associated fibroblasts are activated in incipient neoplasia to orchestrate tumor-promoting inflammation in an NF-kappaB-dependent manner. *Cancer Cell* 17: 135-47
21. Nazareth MR, Broderick L, Simpson-Abelson MR, Kelleher RJ, Jr., Yokota SJ, Bankert RB. 2007. Characterization of human lung tumor-associated fibroblasts and their ability to modulate the activation of tumor-associated T cells. *J Immunol* 178: 5552-62
22. Ali SR, Ranjbarvaziri S, Talkhabi M, Zhao P, Subat A, Hojjat A, Kamran P, Muller AM, Volz KS, Tang Z, Red-Horse K, Ardehali R. 2014. Developmental heterogeneity of cardiac fibroblasts does not predict pathological proliferation and activation. *Circ Res* 115: 625-35
23. Patriarca C, Macchi RM, Marschner AK, Mellstedt H. 2012. Epithelial cell adhesion molecule expression (CD326) in cancer: a short review. *Cancer Treat Rev* 38: 68-75
24. Sugimoto H, Mundel TM, Kieran MW, Kalluri R. 2006. Identification of fibroblast heterogeneity in the tumor microenvironment. *Cancer Biol Ther* 5: 1640-6

4. IMPACT

What was the impact on the development of the preliminary discipline of the project? The results at this point suggest that tumor SHG F/B ratio may be used as an early indicator of metastatic risk.

What was impact on other disciplines, technology transfer, and on society beyond science and technology? Nothing to report.

5. CHANGES/PROBLEMS:

Nothing to report in any area.

6. PRODUCTS:

Publications, conference papers, and presentations:

Madden, K.S., Dawes, R.P., D.K. Byun, E.B. Brown. 2014. β_2 -Adrenergic Agonist Treatment Inhibits 4T1 Breast Tumor Metastasis to the Lung. Annual Psychoneuroimmunology Research Society Scientific Meeting, Philadelphia, PA. (Oral Presentation)

No website, technology, inventions, patent applications, licenses, or other products to report.

7. PARTICIPANTS & OTHER COLLABORATING ORGANIZATIONS:

Individuals who have worked on the project:

NAME: Kelley S. Madden, PhD

Project role: PI

Researcher identifier: ?

Nearest person month worked: 6

Contribution to project: Dr. Madden has planned and designed all experiments. She has assisted with the execution of these experiments. She has analyzed all results.

NAME: Daniel Byun

Project Role: Technician

Researcher Identifier: ?

Nearest person month: 10

Contribution to project: Mr. Byun has executed all aspects of the *in vivo* experiments. He has also assisted with data analysis.

NAME: Eugenia Zeng

Project Role: Undergraduate Student

Researcher Identifier: ?

Nearest person month: 1

Contribution to project: Eugenia executed all experiments isolating tumor associated fibroblasts

NAME: Seth Perry, PhD

Project Role: co-investigator

Researcher identifier: ?

Nearest person month: 1

Contribution to project: Assisted with isolation of tumor associated fibroblasts and with SHG image analysis.

No change in the active support of the PI or senior/key personnel since the last reporting period.

No other organizations were involved as partners.

APPENDICES: None